Technical Report No. 32-669

An X-ray Spectrograph for Lunar Surface Analysis

Albert E. Metzger

JET PROPULSION LABORATORY
CALIFORNIA INSTITUTE OF TECHNOLOGY
PASADENA, CALIFORNIA

October 16, 1964

Technical Report No. 32-669

An X-ray Spectrograph for Lunar Surface Analysis

Albert E. Metzger

C Thiele

Carl Thiele, *Chief*
Applied Science Section

JET PROPULSION LABORATORY
CALIFORNIA INSTITUTE OF TECHNOLOGY
PASADENA, CALIFORNIA

October 16, 1964

Prepared Under Contract No. NAS 7-100
National Aeronautics & Space Administration

CONTENTS

TABLES

FIGURES

FIGURES (Cont'd)

ABSTRACT

15407

The potential of X-ray spectroscopy for the remote elemental analysis of lunar and planetary surfaces has been explored. This Report describes the performance of a proposed X-ray Spectrograph for the in situ analysis of powdered samples of lunar material.

General considerations in the design of the X-ray Spectrograph for lunar analysis are discussed. The instrument employs electron beam excitation, with dispersive crystal resolution in a fixed channel geometry. A nondispersive capability by means of pulse height analysis is also included. Stable X-ray emission has been achieved by lowering the electrical resistivity of the sample. Thermal measurements show that heating of the sample by the electron beam is not excessive. Variations in particle size and shape have been found to affect the response, but these become serious only in extreme cases. The processes of interelemental X-ray absorption and enhancement are discussed, and are illustrated by curves of response as a function of composition.

Experimental results using both synthetic and natural rock materials are presented for the dispersive and nondispersive modes. It is concluded that X-ray spectroscopy can be adapted to lunar spacecraft operation to perform a straightforward quantitative analysis for elements present in minor as well as major abundance.

author

I. EMISSION AND DETECTION OF X-RAYS

The interaction of either an electron or an X-ray quantum with an orbital electron can remove the orbital electron from its atom. The resultant vacancy will be filled by an electron from an outer shell of the same atom. This transition to a lower energy level is accompanied by the emission of an X-ray whose energy is defined by the initial and final electron state. Transition energies vary in a systematic manner with atomic number, and it is this relationship which provides the basis of X-ray fluorescence spectroscopy.

Characteristic X-ray emission line spectra can be resolved according to wavelength by either electronic or optical discrimination. Optical discrimination requires

the use of analyzing crystals to diffract a particular wavelength according to Bragg's law, $n\lambda = 2d \sin \theta$, where

λ is the wavelength of the X-ray

d is the interplanar spacing of the diffracting crystal

θ is the angle between the X-ray and the crystal plane (Fig. 1).

A collimating stack of parallel blades or tubes is inserted either between the X-ray source and analyzing crystal, or between the analyzing crystal and an X-ray detector. For a parallel beam incident on the crystal, only those X-rays which satisfy the Bragg equation for a given wavelength or higher integral orders of n will be diffracted through the collimator stack. By fixing the value of θ through geometrical orientation it is possible to define the one wavelength (irrespective of higher orders) which will be diffracted.

Electronic discrimination, commonly called nondispersive analysis, dispenses with both crystal and collimator, and instead relies on a radiation detector which produces an output signal proportional to the X-ray energy deposited in it. After suitable stages of amplification, the signal undergoes pulse height analysis. The counting of a statistically significant number of events produces a spectrum of energy versus intensity. Optical and electronic discrimination can be used together if desired.

An X-ray flux can be detected by a scintillation or proportional counter, both of which produce the energy dependent output signal necessary for pulse amplitude discrimination, or by a Geiger counter whose output pulse amplitude is independent of the ionizing event. Solid state detectors offer future promise. Most K series lines are easily detected by conventional proportional and Geiger counters; however, the limited range of characteristic X-rays from light elements presents the problem of transmitting a significant fraction of the flux through the counter window and to the sensitive portion of the counter. Absorption losses can be minimized by the establishment of a low density path between the source of X-rays and the counter, the thinnest possible counter window, and a minimum of dead space in the counter itself.

The output of an X-ray tube will excite fluorescent radiation of lower energy. These secondary X-rays are predominantly characteristic line spectra, with little nonline background accompanying them. A beam of electrons is a much more efficient method of generating X-ray emission from a sample. However, when electrons are used for excitation, the characteristic X-ray lines are superimposed above a substantial continuous spectrum generated by the deceleration of electrons in the target. Both types of excitation are currently employed in laboratory instruments, secondary excitation in conventional X-ray spectrometers, and primary excitation in the recently devised electron microprobe which can focus a beam of electrons no more than a micron in diameter on a specimen under investigation.

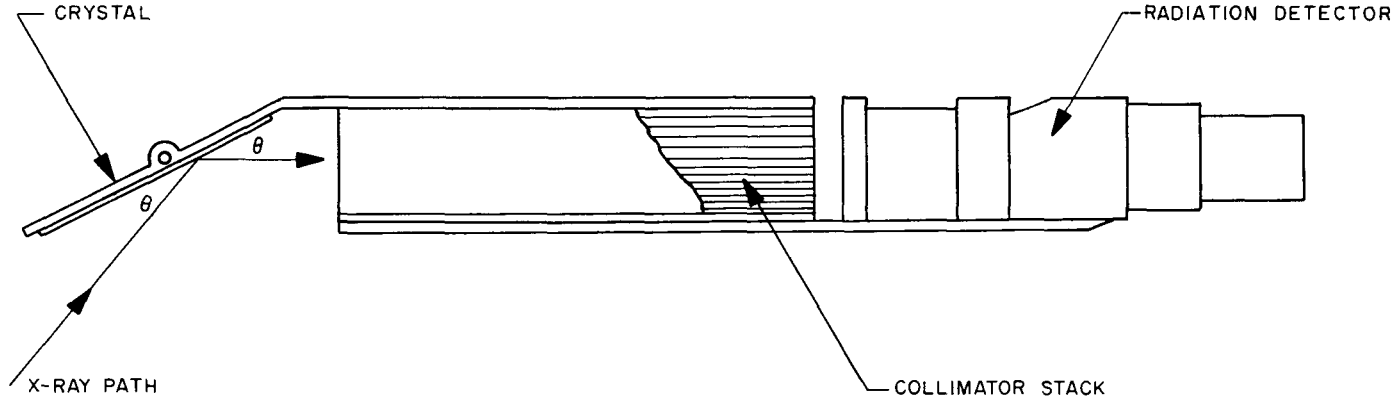

Fig. 1. Optical discrimination of X-rays

II. LUNAR INSTRUMENT DESIGN

The use of an X-ray spectrograph as a means of performing in situ elemental analyses on powdered samples of lunar material was proposed by Philips Electronics Instruments (PEI) Inc. of Mt. Vernon, New York as part of the *Surveyor* Program for soft lunar landings of unmanned spacecraft. The design which emerged from their feasibility study reflected three significant decisions which are discussed in the following paragraphs (Ref. 1).

The sensitivity of any analytical technique is dependent on the degree to which the desired signal can be discriminated from other signals and from any background which may be present. Analyzing crystals and collimators were chosen as the primary means of wavelength discrimination because the resolving capability of a dispersive system is at least an order of magnitude greater than the nondispersive combination of proportional counter and pulse height analyzer. This offsets the greater intensity of response in the nondispersive system for identical conditions of excitation. The lower intensity of dispersive analysis stems from the inefficiency of the diffracting crystals and losses in the collimator stack.

The use of a beam of electrons for sample excitation rather than radiation from a suitably designed X-ray tube was based on power limitations for spacecraft operation. At a given power level, electron excitation will produce an intensity of response several orders of magnitude greater than that produced by fluorescent excitation. The fact that the required vacuum is a characteristic of the lunar environment makes it possible to use electron excitation without extreme design problems. The continuous spectrum which accompanies electron excitation adds to the advantage of dispersive over nondispersive analysis.

A third major decision was the choice of a multiple fixed channel geometry rather than a scanning system. Instead of providing individual channels for each element, a single goniometer assembly is capable in principle of scanning through the entire range of elements by continuously varying the Bragg angle. A scanning system requires fewer components for dispersion and detection. Scanning also provides additional X-ray lines and a more complete pattern of the continuum to assist in the interpretation of the data. However, the advantages of a fixed system are considerable and, for this application, outweigh those of the scanning system. Simplicity in the form of a single crystal and detector is obtained at the cost of mechanical complexity in the design and operation of a moving system which must be maintained in angular alignment over its entire scanning range. Redundancy is diminished. The loss of crystal or collimator alignment, or the failure of a detector, which for the fixed system might be confined to one element, would, in the case of scanning, eliminate the entire experiment. The response characteristics of a scanning system would necessarily represent a compromise over the wavelength range without the chance to "tune" each channel for maximum sensitivity by the appropriate choice of crystal, collimator, and detector. This capability is especially useful for the lower atomic number elements. Finally, the fixed system is capable of making an analysis in a fraction of the time required to obtain equivalent counting statistics by scanning.

The outcome of these considerations was the design of the Lunar X-ray Spectrograph[a] as a fixed channel system with provision for both dispersive and nondispersive wavelength resolution, employing electron bombardment for sample excitation. Since the delivery of a breadboard instrument, X-ray fluorescence spectroscopy has been studied extensively at the Jet Propulsion Laboratory (JPL) in order to assess its suitability for lunar surface analysis. This Report deals with investigations into sample behavior under electron bombardment, particle effects, matrix interactions, and the analysis of rocks. A subsequent article will review the design studies which have been performed to optimize the functional capability of the instrument.

[a] Common usage variously refers to this type of instrument as an X-ray spectrograph and as an X-ray spectrometer. The lunar device has been a victim of this ambiguity. It is an X-ray spectrograph in this Report, primarily because the model used in this work has always been so designated, and partly because this minimizes confusion with nondispersive systems which are generally termed X-ray spectrometers.

III. DESCRIPTION OF INSTRUMENT

The breadboard instrument constructed by PEI is shown schematically in Fig. 2. The electron gun consists of a heated tungsten filament, a control grid for focusing the electron beam, and an anode. The filament is biased to negative high voltage, the control grid is operated at 50–100 v positive with respect to the filament, and the anode is at ground potential. The electron gun projects a beam of electrons through the hollow anode onto a target surface in the shape of a slightly elliptical spot. Fluorescent radiation from the excited sample is viewed by 13 dispersive channels, each channel corresponding to a selected element of geochemical interest. These range from sodium to nickel and are listed in Table 1. A dispersive channel consists of a crystal positioned at the reflection angle θ for the appropriate wavelength, a flat bladed collimator stack which defines the acceptance width $\Delta\theta$ of the diffracted X-rays, and a radiation detector (Fig. 1). The crystals used in these tests have been sodium chloride, EDDT, and potassium acid phthalate. Geiger counters are used for elements of atomic number 16 and above, proportional counters for the lighter elements. Output pulses from the proportional counter are passed through a double threshold circuit to improve discrimination against such contributions to the background

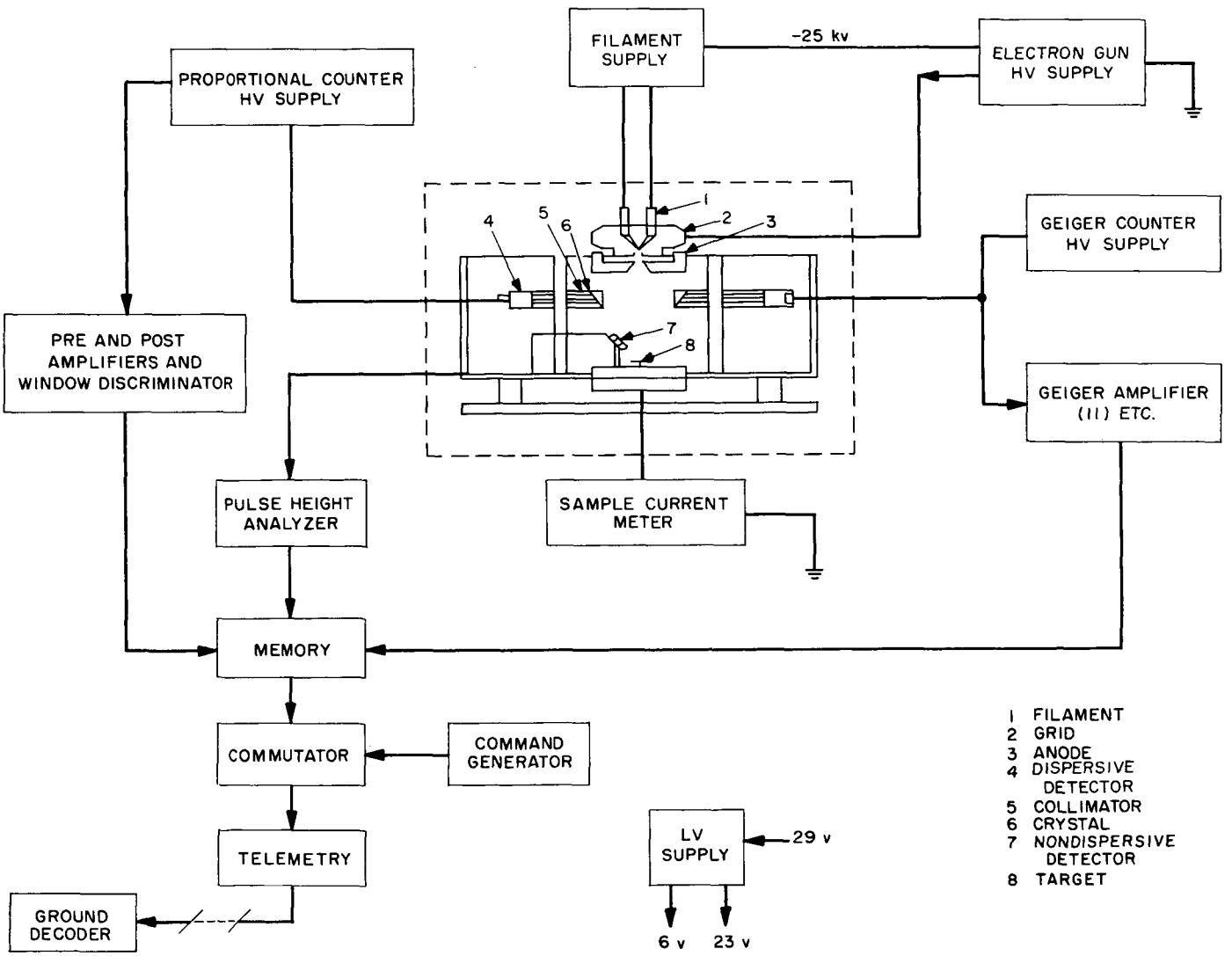

Fig. 2. Schematic of the Lunar X-ray Spectrograph

Table 1. Lunar X-ray Spectrograph dispersive channel capability

Z	Element	Z	Element
11	Sodium	22	Titanium
12	Magnesium	23	Vanadium[a]
13	Aluminum	24	Chromium
14	Silicon	25	Manganese
16	Sulfur	26	Iron
19	Potassium	28	Nickel
20	Calcium		

[a]To be replaced by a chlorine channel

as the X-ray continuum, scattered radiation, higher orders of reflection from the analyzing crystals, and fluorescence induced in the crystal by radiation from the target. A separate nondispersive proportional counter views the sample directly. Its amplified output is transmitted to an analog to digital converter for pulse height analysis. The nondispersive system provides a backup to the dispersive channels for elements of major abundance, and also guards against the possibility, however unlikely, that an abundant element will be encountered for which no dispersive channel has been provided.

The planned integration of the instrument with the *Surveyor* spacecraft included sufficient memory stages of buffer storage for the dispersive and nondispersive outputs to be compatible with the bandwidth available for transmission. The readout of information from the memory to telemetry would be accomplished by a commanded commutator system. Although the Geiger counters, proportional counters, and electron gun require different voltages for operation, one high voltage supply can be used if separate secondary windings and circuits for regulation and noise suppression are provided.

IV. TEST CONDITIONS

The portion of the breadboard which has been operated in the vacuum is shown within the dotted line of Fig. 2. A pressure of 5×10^{-5} mm is low enough for long-lived filament emission. The low voltage power supply and output signal electronics have been operated outside the vacuum system for reasons of space and accessibility. Laboratory high voltage supplies have been used for the electron gun and radiation counters. Counts from the dispersive channels have been accumulated in scalers, while a commercial pulse height analyzer has been used for spectral resolution in the nondispersive channel.

Figure 3 shows the breadboard instrument mounted in the vacuum test facility. Prominent in the foreground are the three high voltage supply feed-throughs for the filament and grid of the electron gun. The high voltage supply for the electron gun was modified by the manufacturer, Universal Voltronics, to allow operation in either a current regulated or unregulated mode. The energy of the electron beam, its intensity, and its projected area are all controlled independently and can be varied in small increments. The range of experimental operating conditions has spanned an accelerating potential of 5–30 kv, a beam current of 1–200 μa, and a beam diameter of 1/32–1 in. Severe arcing was a frequent occurrence during the first months of testing, but with improvements in the high voltage connections, a stable power supply, and a clean vacuum chamber, such transients have been eliminated from normal operation.

The sample tray is visible below the electron gun. It can accommodate up to 12 samples. These are positioned under the gun as desired by a mechanical arm and sprocket system. The flow counter seen in Fig. 3 was installed for the purpose of comparing various filling gases during a series of design tests.

Operation of the instrument presents no radiation health hazard. The only special precaution taken was the installation of lead glass in the viewing port of the vacuum chamber.

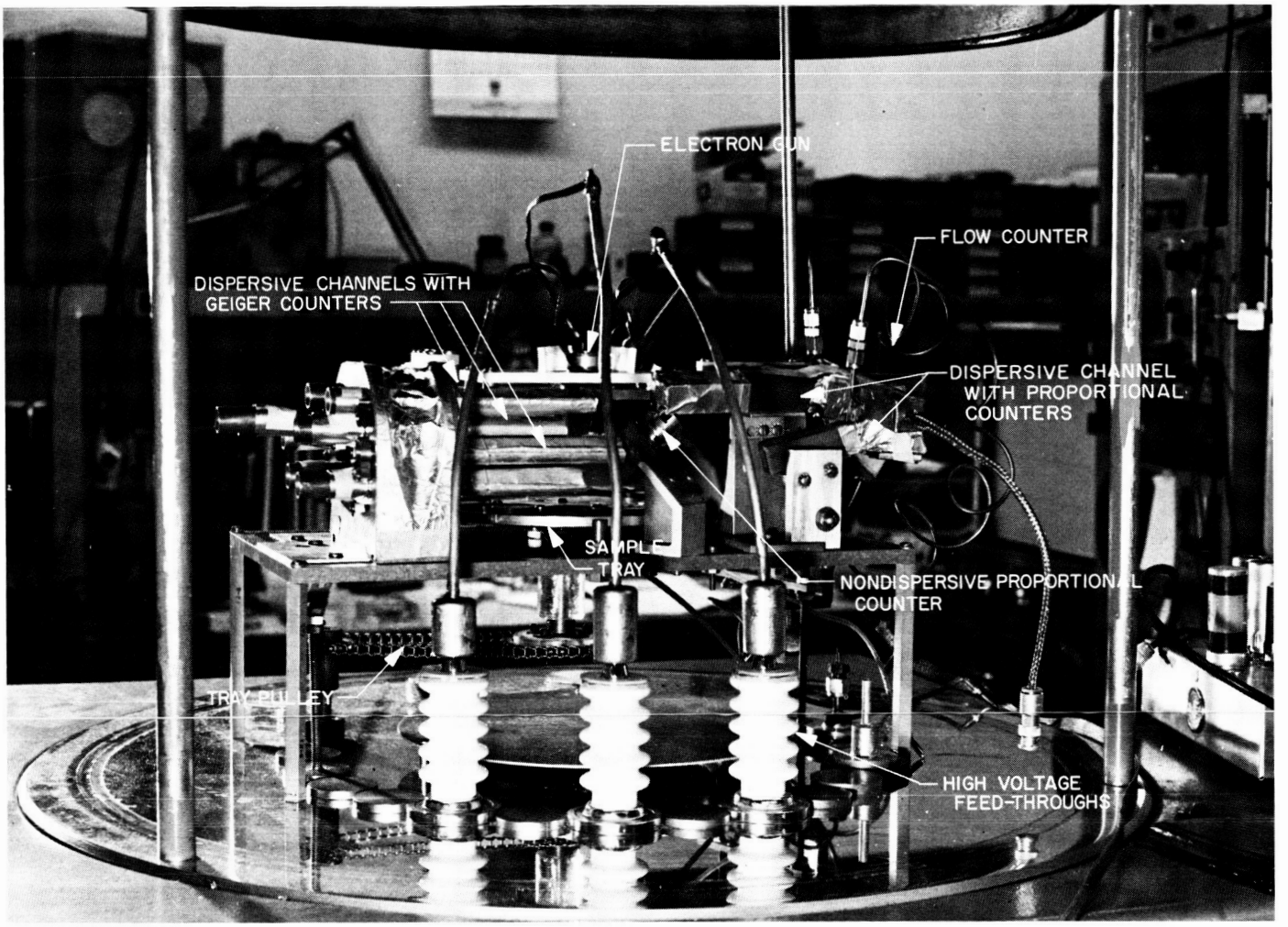

Fig. 3. Lunar X-ray Spectrograph breadboard model

V. STANDARD SAMPLES

An early test objective was the choice of a simple chemical compound for each element that the Spectrograph was designed to detect dispersively. This was done to obtain reference compounds for use as calibration standards. Another objective of at least equal importance was to study the response characteristics of a variety of powders to electron beam bombardment, since the instrument has been designed to analyze pulverized samples. Altogether, some 30–35 powders with promising physical properties were exposed to the electron beam under rapidly changing conditions of excitation and for prolonged bombardment times. Powders which have a low melting point or dehydration temperature are not suitable, while those which are hydroscopic are difficult to store over long periods of time. Any preconditioning of these powders, such as baking at elevated temperatures, has been avoided as impractical for lunar operation. The compounds selected as reference standards are listed in Table 2. Several are best compromises rather than ideal in their behavior.

Table 2. Compounds for X-ray spectrograph testing

Channel	Compound
Na	NaF
Mg	MgO
Al	Al_2O_3
Si	SiO_2
S	Li_2SO_4
K	K_2CO_3
Ca	CaO
Ti	TiO_2
V	V_2O_5
Cr	Cr_2O_3
Mn	MnO_2
Fe	Fe_2O_3
Ni	NiO

An effect which is evidently due to the surface adsorption of gases has been observed with powdered MgO. The intensity of X-ray emission rises gradually from the start of operation and finally equilibrates with a 25% increase over a 30-min period. Maintaining the vacuum system at constant pressure demonstrated that the increase in intensity cannot be due to a decrease in absorption between the sample and the detector. The effect has not been observed with any other material.

VI. SAMPLE CONDUCTIVITY

Sudden transients in the electron beam flux can produce damage at the surface of many powdered samples, ranging from minor pitting to volcanic-like bursts of material. The integrity of a target surface was found to depend on the rate of rise of both the electron gun voltage and the electron gun current. This was particularly true of materials which are poor conductors. In almost every case damage could be eliminated by extending the rise for 30 sec or longer. Once the nominal operating conditions were reached and stable conditions of excitation prevailed, the surface integrity remained intact indefinitely.

When the fluorescent emission from several reference powders was examined as a function of gun current, a pattern such as that shown schematically in Fig. 4 for ferric oxide was observed. As the gun current is increased, the counting rate first rises proportionately, then decreases as a space charge of electrons builds up at the target surface. The count rate remains low with occasional sharp fluctuations, until a point is reached at which the kinetic energy of the electron flux has heated the sample sufficiently to lower its resistivity. The sample begins to conduct, the space charge disappears, and the counting rate rises dramatically. For confirmation, an

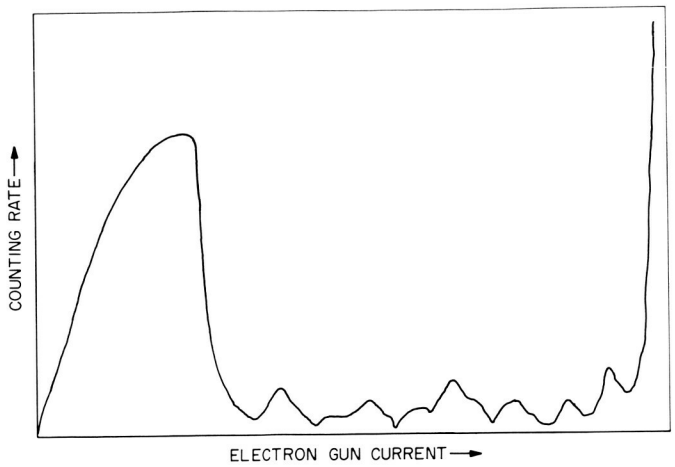

Fig. 4. Response of a nonconducting powder to increasing electron gun current

ammeter was placed in series with the ground return from the sample tray to monitor the sample current (Fig. 2). It showed the same pattern of behavior observed for the count rate response.

Since intensity and stability became satisfactory only when the operating conditions were such as to sensitize the sample to a state of relative conductivity, higher power levels were applied in an unsuccessful effort to achieve a standard operating condition for which all nonconducting samples would respond adequately. However, the beam energy per unit area required for this proved to be impracticably high. In addition, long term count rate drifts were found which could not be eliminated. The next effort consisted of an attempt to provide a discharge path for the electron beam by means of a 40-mesh brass screen placed across the top of the graphite

Fig. 5. Fixture for measurement of sample resistivity

cup containing the sample, or alternately by embedding a 25-mil copper pin in the center of the cup. Both methods eliminated gross charging at the target surface. A series of tests showed that the pin provided better stability than the screen, occupied a smaller area, and contributed surprisingly little to the background intensity. It appeared possible to incorporate this pin in the sample cup without affecting the proposed spacecraft sample preparation system. It was pointed out that the copper pin could also serve as a calibration standard (Ref. 2).

The discharge pin was used for several months. However, as analytical work became more quantitative, repetitive measurements showed deviations that could not be tolerated. Short and long term drifts were still present, though less pronounced with the use of the pin. An early attempt to make the target surface uniformly conductive by spraying on a thin layer of powdered graphite had failed as the graphite simply vanished under the electron beam due to electrostatic repulsion. However, when a quantity of powdered graphite was uniformly distributed throughout the sample, the improvement in stability was dramatic. Measurements with an ohmmeter placed in series with sample material (Fig. 5), showed that the addition of 5–15% of graphite lowered the electrical resistivity of nonconducting materials by five to seven orders of magnitude. Some of the results are given in Table 3. Apart from special purpose tests, all powdered specimens now contain a fixed quantity (usually 15%) of added graphite. Good sample conductivity has produced other benefits. The linearity of X-ray response to increasing beam current has improved. Furthermore, there is no longer any limitation on the rate of rise of gun current or voltage in order not to disturb the sample surface. There is therefore no need for any built-in electronic delays when the instrument is turned on.

Table 3. Effect of graphite on the resistivity of certain nonconducting powders[a]

Sample	Sample Measurement	Added carbon, % 0	1	5	10	15	20
SiO_2	Resistivity, Ω	85 meg.	∞	∞	43	3.6	0.55
	Sample current, μa	3	1.4	18	20	20	20
CaO	Resistivity, Ω				1000 meg.	38	1.5
	Sample current, μa				4.2	19	19+
K_2CO_3	Resistivity, Ω				420	0.55	
	Sample current, μa				20	20	

[a] Operating conditions: 25 kv beam voltage — 20 μa beam current

Good conductivity in lunar samples could be obtained by simply precharging the sample mixing chamber with a small known quantity of a suitable material such as graphite. The use of a low voltage discharge device has been proposed as an alternate approach (Ref. 3). A limited number of tests were performed with a copper ring, about 3/4 in. in diameter, positioned 1/4 in. above the sample. The ring was biased 100v positive with respect to the sample. The results suggest that this approach can only supplement, but not replace, conductivity in the target for the beam intensities under consideration (5–50 μa). Reference to Fig. 4 indicates that nonconducting sample operation may be possible at beam currents low enough to avoid building up the negative space charge. Such current levels would be 1–2 orders of magnitude below those now in use, so that a loss of sensitivity and a considerable sacrifice in the speed of analysis would be involved.

VII. TARGET TEMPERATURE

Bombardment by 3×10^{14} e/sec (50 μa) with an average energy of 25 kev delivers approximately 10^7 erg/sec of energy to the target, much of which must be dissipated as heat. If elevated temperatures are developed in the sample, the more volatile constituents of certain rock types, such as SO_2 and Cl_2, may be driven off. In order to determine if standard operating conditions produce an unacceptable level of sample heating, the temperature at the surface of a powdered target has been measured as a function of beam flux and spot size. A thermocouple was embedded in a 200-mesh sample of granite with its sensitive area just clear of the powder. Holes were drilled in the base of the sample cup to accommodate the thermocouple leads. The electron beam was passed across the thermocouple by rotating the sample holder tray until a maximum reading was obtained. When this point was located, the thermocouple was allowed to sit under the beam for 1 min to assure that equilibrium had been reached. The most reliable set of results is shown in Table 4. Note that for the maximum electron flux to be used in analysis, 25 kv, 50 μa and a spot diameter of 3/16 of an inch, the temperature was 234°C, removing any cause for concern about overheating.

Table 4. Thermocouple measurements of beam spot temperature on a powdered granite target [a]

Current, μa	Temp., °C		
	1/4 in.[b]	3/16 in.[b]	1/8 in.[b]
5	47	51	68
10	56	68	87
20	73	103	129
30	85	154	177
40	104	197	221
50	123	234	274
100	213	402	483

[a] Operating condition — 25kv.
[b] Spot size

VIII. SPECIMEN PRESENTATION

A. Procedure

Material for powdered samples is prepared by grinding as necessary, followed by sifting to eliminate particles above a given size. The sample is prepared according to the appropriate weight percentages, and mixed by shaking and tumbling in a plastic vial. A graphite cup with a cavity 1/16 in. deep and 1-1/8 in. in diameter is filled with an excess of powder. The powder is leveled off and compressed with a flat metallic surface. Excess powder is simply decanted, and the specimen is ready for use.

The possibility of preferential sorting during grinding, shaking, or tumbling has been investigated for five sample mixtures representing a variety of particle characteristics. Specimens were prepared from the top, middle, and bottom of each mixture, and the respective intensities were measured on the Spectrograph. The percentage spread in response for each set of specimens is given in Table 5 together with the procedure used for mixing. The criteria for sample segregation is considered to be a variation in response for any specimen of a set greater than a 2σ deviation from the mean of that set. Segregation occurred for all samples which were mixed only by machine, evidently due to a predominantly horizontal motion in the commercial shaker used. Shaking by hand overcame this deficiency. The distribution of Mn in Al_2O_3 proved obstinate; the highest Mn intensity consistently appeared in the middle fraction. Apart from this example a combination of tumbling and shaking was able to prevent any preferential sorting which would have distorted the analytical results. The importance of such considerations for any spacecraft sample processing system is obvious.

Table 5. Segregation test results

Mixing procedure[a]	Sample	Element observed	Maximum % spread from average	Segregation yes $> 2\sigma >$ no
A	5% Fe . 95% SiO_2	Fe	36	Yes
B			12	No
C			26	No
D			4	No
A	16% MnO_2 . 84% Al_2O_3	Mn	43	Yes
B			28	Yes
C			16	Yes
D			19	Yes
E	16% MnO_2 . 84% SiO_2	Mn	6	No
A	14% CaO . 9% Al_2O_3 77% SiO_2	Ca	30	Yes
B			3	No
A	84% Al_2O_3 . 16% MnO_2	Al	10	Yes
B			10	Yes
C			5	No
D			8	No

[a] A Machine shaken
B Machine shaken, then handshaken
C Tumbled 10 min
D Machine shaken, handshaken, then tumbled
E Tumbled, then handshaken

B. Compaction and Surface Smoothness

Even with the conductive filler a moderate amount of surface compaction has been found to be necessary to preserve the surface integrity of powdered targets under electron bombardment. A pressure of 5 psi is sufficient in most cases.

The principal effect of compaction, particularly at low pressures, is to improve the surface smoothness of the target. As surface irregularities are reduced, the effective path length of the emergent X-rays decreases so that absorption losses are reduced. Because absorption increases with the wavelength, the sensitivity to changes in surface smoothness are expected to increase with the wavelength of the characteristic X-ray.

In order to study the effect of compaction on the intensity of X-ray emission, a mechanical fixture has been constructed which allows close control of compaction pressure. The screw and gauge device shown in Fig. 5 allows any pressure between 1 and 50 psi to be applied to a sample in preparation. A hydraulic press is used for higher pressures. Figure 6 shows the variation in the intensity of response for iron and aluminum over a wide range of compaction pressures. The intensity from powdered iron increases less than 8% from 5–25 psi, while the increase for aluminum oxide is 30% from 5–1000 psi. A separate test with fewer measurements gave an increase of roughly 10% for iron from 10–1000 psi. The observation that the effect is smaller for iron

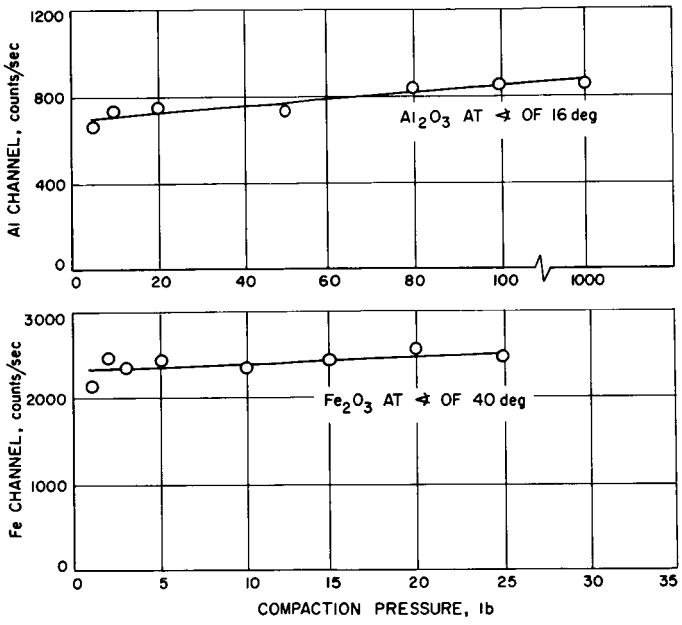

Fig. 6. Effect of compaction on count rate response for X-rays of short and long wavelength

than for aluminum is in agreement with the prediction made on the basis of the difference in wavelength. However, even at the comparatively long wavelengths of aluminum, Fig. 6 shows that the response of the powdered specimen is relatively insensitive to changes in compaction pressure in the 10–25 psi range. If this were not the case, the ability to obtain quantitatively reproducible results would be seriously limited.

A second factor involved in determining the effective path length of fluorescent radiation is the take-off angle, defined as the angle which the emitted radiation makes with the surface of the sample. The take-off angle for the dispersive analysis of aluminum in the breadboard is only 16 deg. A modification of the sample tray was made to allow a sample cup to be inclined at any angle to the dispersive channels. On repeating the compaction test for aluminum radiation at a take-off angle of 46 deg, the effect of pressure on intensity was found to be only one-half as great as at 16 deg (Fig. 6). The avoidance of low take-off angles can remove any excessive dependence of intensity on surface condition at long wavelengths. This subject will be discussed more fully in the forthcoming article on design.

C. *Consolidated Targets*

Although the Lunar X-ray Spectrograph was designed for the analysis of powdered samples, preliminary tests have been made into the response characteristics of nonconducting consolidated targets, using a painted aquadag trail or metal finger to provide a discharge path for the electron beam. Stable fluorescent emission has been obtained from rock samples as well as from a piece of glass. The irradiation of surfaces of varying roughness will determine how much analytical capability can be retained if sample processing is eliminated. The need for accurate alignment between crystal and sample will almost certainly make direct deployment impractical for a dispersive system; this limitation is much less stringent for a nondispersive system.

IX. EFFECTS OF HETEROGENEITY

A sample of iron powder prepared from a batch screened to a maximum particle size of 75 μ produces an intensity of response within 3% of that from an iron disc. Iron powder drawn from the same batch and prepared as a 5% sample in SiO_2 produces a response proportional to its concentration. Let this same batch of iron powder be ground for 30 min or more and the tests repeated; the sample of 100% powder will be unaffected by the grinding, but the response of the 5% sample will be found to have more than doubled!

This curious behavior is symptomatic of the difference in response between homogeneous and mixed samples, and the role which particle shape, as well as particle size, plays in contributing to the difference. Such effects have been discussed in a paper by Claisse and Sampson (Ref. 4), and although their study was done for fluorescent excitation, tests with the Spectrograph have shown that these particle effects also exist with electron excitation. The observed intensity will be determined by the effective particle diameters traversed through both fluo-

rescent and nonfluorescent particles by radiation of the fluorescent element to be detected, or in other words, on the relative volume concentrations of the phases, which depend on the size and shape of the grains making up the mixture.

Iron powder and ferric oxide have been used extensively to study these particle effects with the breadboard. The iron powder is very granular and irregular in shape, the ferric oxide is finely divided and tends to spherical clumping (Fig. 7). It is believed that this pair represents at least as extreme a range of particle types as is likely to be encountered in actual rock analysis.

When the mean particle size is sufficiently large, the X-ray intensity is linearly proportional to concentration. This is the case for the unground iron powder mixture mentioned above. It has also been found to be true for a 5% ferric oxide sample prepared with a minimum of mixing. When the ferric oxide sample is thoroughly shaken however, the reduction in mean particle size distributed through the silica produces a nonlinear enhancement of iron fluorescence. That these results were not due to incomplete or preferential mixing was demonstrated by running segregation tests of the type described in Section VIII on both the minimally and thoroughly mixed ferric oxide samples.

Grinding, rather than mixing, is required to reduce the particle size of the hard particles of iron powder. The fluorescence of 5% mixtures prepared from powder ground for varying periods of time reached a maximum only after approximately 1 hr of grinding, with an intensity almost twice the initial value. As a check, iron powder was ground as a 5% mixture with silica and sampled over a 3-hr grinding period. The degree of enhancement was reduced by almost a factor of 10, due to dilution of the selfabrasive action of the powder grains.

To strengthen the conclusion that these are physical effects of grain size rather than chemical composition, ferrous sulfide samples were subjected to mixing and grinding tests. Ferrous sulfide has a granular structure similar to powdered iron. Test results showed good quantitative agreement with powdered iron.

This low concentration enhancement effect develops as particle size becomes small in relation to the range of the X-ray involved. Since the range of characteristic X-rays decreases with decreasing atomic number, particles of a given size will look larger to X-rays as the

(a) Fe_2O_3 (100X)–UNGROUND

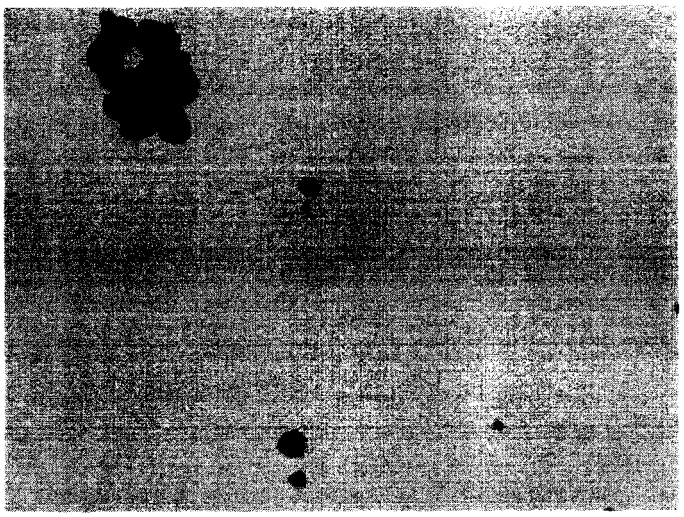

(b) Fe POWDER (100X)–UNGROUND

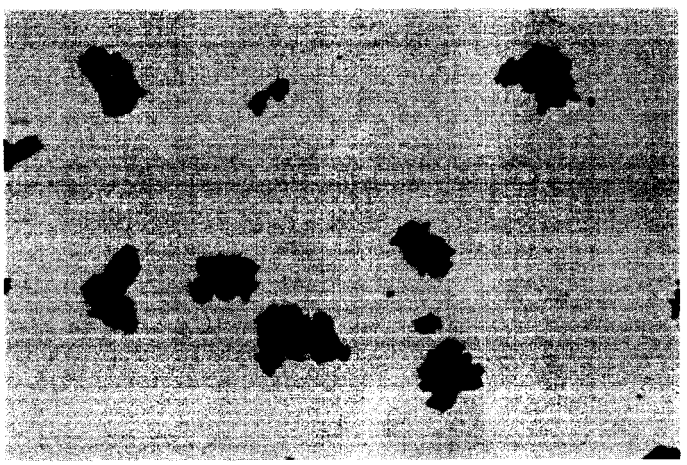

(c) Fe POWDER (100X)–3-hr GRIND

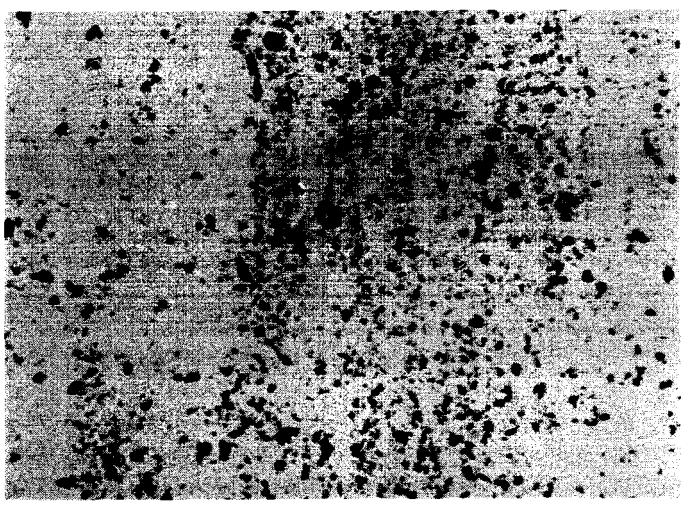

Fig. 7. Iron and iron oxide powders used in heterogeneity studies

limit of sensitivity for rock analysis will be about 0.05% for most elements.

B. Nondispersive Analysis

The capability of the nondispersive channel to provide quantitative information has been tested with the breadboard by first obtaining the spectral distribution of a set of elements and standards, and then rerunning the same specimens additively under the same conditions to produce composites. Two examples of such composite pulse height spectra are shown (Fig. 8 and 9). Note that in Fig. 8 only three X-ray peaks are evident even though the composite has six components. The energy spectrum

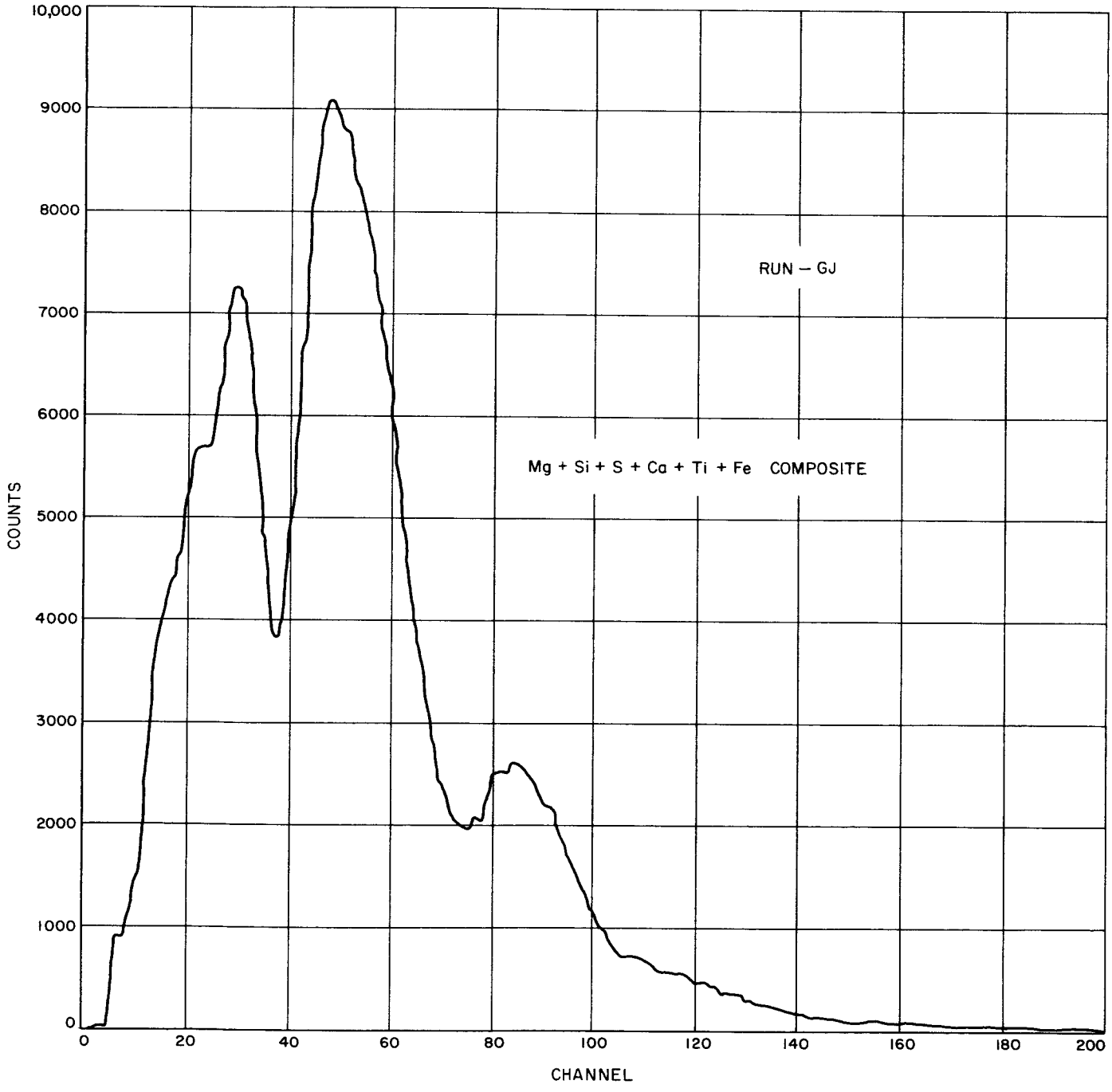

Fig. 8. Six component composite nondispersive pulse height spectrum

wavelength of the X-rays increases. The expectation then, is that for a given mean grain size, the enhancement effect ought to decrease with atomic number. This has been borne out qualitatively in our testing since this enhancement has been observed only for elements of $Z > 22$.

Although a mean particle size of a micron or less can increase sensitivity at low concentrations by the enhancement of fluorescence, it will be better to avoid excessive grinding and operate with a mean particle size which produces a linear response. The linear results with unground iron powder indicate that this can be obtained without going over 75-μ (200-mesh) particles, which still retains a sufficiently smooth sample surface. These heterogeneity effects suggest that calibration standards for the Spectrograph should be analyzed rocks, or if mixtures of chemical compounds, should have particle characteristics similar to rock material. The grinding and delivery mechanisms of any lunar sample processing system must be effective enough to minimize nonlinear responses due to variations in rock hardness.

X. SENSITIVITY

A. Dispersive Analysis

The analytic sensitivity of any channel of the Spectrograph will be determined by its ability to discriminate against the background of unwanted X-rays, by the total number of counts recorded, and by instrumental instabilities. If the last factor is ignored, the lower limit of detection will correspond to the concentration which produces a recognizable signal above the background level, with the word "recognizable" defined by some level of statistical confidence. For comparative purposes in functional and design testing, the performance of both dispersive and nondispersive channels has been referenced to ratios of signal to background intensities, where the signal is generated by a pure element or simple compound, and the background is the continuum produced in that channel by a nickel or copper foil. In the nondispersive case, the signal and background are the total count rates integrated over those pulse height analyzer channels containing the X-ray peak of interest. It is possible to relate these signal to background ratios to the minimum detectable limit by applying equations

$$R_s^c = n_\sigma \frac{[R_t + (R_t R_b)^{1/2}]^{1/2}}{g_{R_s} (t_s)^{1/2}} \quad (1)$$

$$R_s = \frac{C^{100}}{KC} R_s^c \quad (2)$$

where

R_s^c = signal counting rate for concentration c

n_σ = level of statistical confidence

R_t = total (signal + background) counting rate

R_b = background counting rate

g_{R_s} = fractional standard deviation of the sample counting rate

t_s = sample measurement time

K = matrix correction factor

C = concentration of the element under consideration

A derivation is presented in the Appendix.

The application of these equations to experimentally determined intensities has shown that, for all dispersive channels other than sodium and magnesium, detectabilities as low as 0.02% are theoretically possible. If as nonlinear effects become more pronounced, the factor K becomes less than unity, the minimum detectable limit equivalent to a given signal to background ratio will increase. However, the values of K which have been determined by applying Eq. (2) to samples of widely varying concentrations range from 0.7–2.0, a favorable situation for the detection of low concentrations. These and other considerations to be discussed in Sections XI and XII make it seem likely at present that the practical

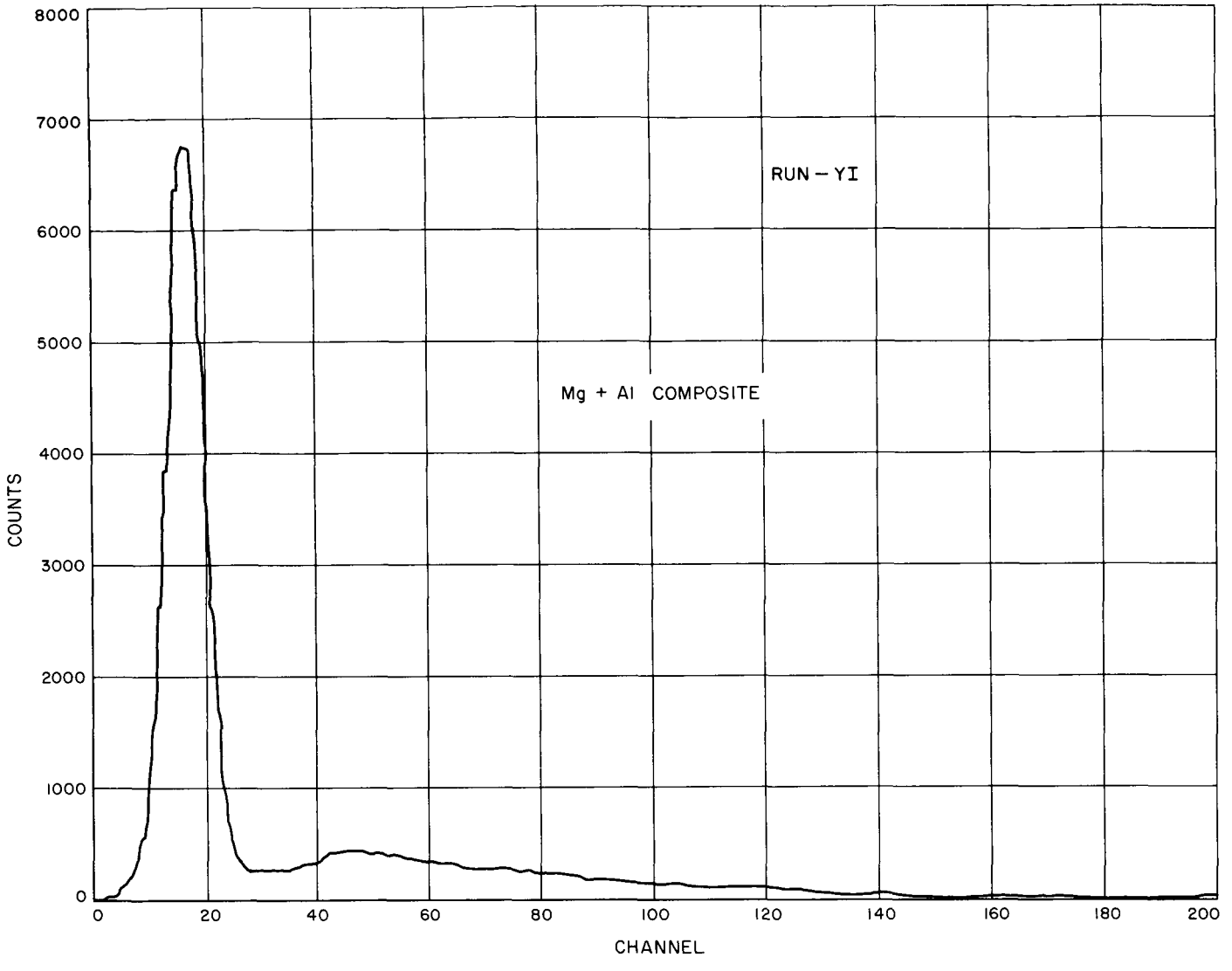

Fig. 9. Two component composite nondispersive pulse height spectrum

of Fig. 9 consists of two components of adjacent atomic number. Such composites have been reduced using computer program techniques of spectrum stripping developed by Dr. Jacob Trombka (Ref. 5). The results for these and other composites are shown in Table 6. The capability of the nondispersive channel to resolve even adjacent elements is surprisingly good. In none of the runs did the nondispersive mode fail to report the presence of an element, and in only two cases (GJ and HJ) did it report a significant amount of an element which was not present. Although these composite tests were entirely independent of sample effects, they indicate that sensitivity levels of 1–3% may be attainable with nonsynthetic targets.

The promising gross analytical capability of nondispersive analysis suggests that it deserves consideration as a separate instrument, less sensitive but lighter than a dispersive X-ray spectrograph. The need to maintain alignment with the diffracting crystals imposes stricter limits on sample position and smoothness in the dispersive case than for nondispersive analysis. The lower level of sample excitation required nondispersively will make it possible to substitute fluorescent excitation for the electron beam. Radioisotopic excitation has also been proposed (Ref. 6). If direct surface excitation proves feasible, a nondispersive X-ray spectrometer could find an important application on the early Apollo missions as a rapid, portable device to aid in the selection of lunar samples for return to Earth. It might also be employed for broad area surface analysis on unmanned roving vehicles.

Table 6. Results of nondispersive composite tests with computer analysis [a]

Run	Mg	Al	Si	S	Ca	Ti	Cr	Mn	Fe	Ni
YI	0.74	1.08	—	—	0.015	0.0023	—	—	—	0.00097
ZI	—	—	1.23	0.83	—	0.0001	—	—	—	—
AJ	—	—	—	—	0.88	1.08	—	—	—	—
BJ	—	—	—	—	—	0.0011	—	—	0.98	1.00
CJ	0.96	—	—	—	—	0.013	—	—	—	0.97
DJ	0.81	—	1.00	0.97	—	0.0064	0.0078	—	—	—
EJ	—	—	—	—	—	0.94	1.16	0.73	—	—
FJ	—	—	0.0055	—	—	—	1.03	—	0.89	1.03
GJ	1.05	—	1.29	0.88	1.08	0.93	—	0.17	0.77	—
HJ	0.57	1.31	0.79	—	1.03	—	—	0.099	0.91	—

[a] 25 KV — 4 μa electron beam. Side window proportional counter — P10 fill

Note: ▒ denotes those elements that made up the composites. If the element is present, the correct relative intensity is 1.00; if absent, —

XI. INTERELEMENTAL EFFECTS

The discussion of heterogeneity in Section IX dealt with sample characteristics and their effect on the response of a single element. This section will briefly describe the sources of interelemental effects, and illustrate the degree to which they have made themselves evident in this program.

The starting point in the application of induced X-ray emission for analysis lies in the simple linear relationship between the weight concentration of an element and the intensity at the point of emission in the specimen,

$$I_A = C_A \times I_{100A} \tag{3}$$

where

C_A = the weight concentration of element A in the unknown

I_A = the emitted intensity of characteristic radiation from element A in the unknown

I_{100A} = the emitted intensity of the characteristic radiation of A from pure A

The effects discussed below occur because the specimens are not infinitely thin. As a result both the incident electrons and the emitted characteristic radiation undergo a number of other processes.

A. Continuum Radiation

The deceleration of electrons in matter due to interaction processes with atomic nuclei will generate a continuous spectrum of radiation. The minimum wavelength of this radiation will be determined by the maximum energy of the electron beam. The peak intensity of the

continuous spectrum will be at a wavelength approximately 1½ times the minimum wavelength. The wavelength which corresponds to maximum intensity is therefore independent of the target material, but the intensity of this background increases with the mean atomic number of the target. The nondispersive channel will see the entire continuum, a dispersive channel will see that portion which falls within its increment of wavelength resolution.

B. Absorption

When X-rays pass through matter, they are subject to absorption according to the exponential relation

$$I/I_0 = e^{-\mu\rho d} \tag{4}$$

where

I_0 = incident intensity

I = transmitted intensity

μ = mass absorption coefficient

ρ = density of the absorber

d = thickness of the absorber

In the case of the Spectrograph, X-rays emitted at finite depths in the target may be absorbed before reaching the surface. The probability of absorption will depend upon the distribution in depth of the X-rays produced in the target, the takeoff angle of the radiation θ, and the absorption coefficient of target material for the radiation wavelength of interest μ_λ. The last two factors take the form of

$$X = \mu_\lambda \csc \theta$$

The parameter X has been included in a function F(X), which includes a term for the excitation as a function of penetration. The penetration will be determined by the energy and angle of incidence of the electron beam, as well as by the composition of the target (Ref. 7). Theoretically and experimentally derived curves of F(X) and X are available for making appropriate absorption corrections (Ref. 8 and 9).

C. Secondary Emission

Both characteristic and continuum radiation generated by electron bombardment may in turn produce additional X-ray emission at longer wavelengths. The effect is to enhance the intensity of the element under study.

Castaing has treated the case of secondary emission caused by the continuum by calculating a single mean wavelength as an approximation to the continuum, and applying this factor to an expression which includes the effective atomic number of the sample, as well as the mass absorption coefficients of both the mean exciting radiation and the characteristic radiation being measured (Ref. 10). The enhancement is expected to be small.

The more important effect of secondary emission due to characteristic radiation becomes significant when the exciting radiation is of only slightly shorter wavelength than the radiation to be measured, and the element giving rise to the exciting radiation is present in large concentration compared to the element under analysis. The various analytical expressions which have been developed for this effect are quite complex (Ref. 11); they include terms for the fluorescence yield, the mass absorption coefficient, the distribution of primary emission with depth, the ratio of absorption edge frequencies for the exciting and excited elements, and the mass per unit volume of the element being excited.

D. Atomic Number

In the discussion of absorption, it was mentioned that the depth distribution of X-rays is related to the composition of the sample. Two phenomena are involved, electron mass penetration (sample stopping power) and electron back-scattering, both of which are dependent on atomic number. Although these two effects tend to cancel, the effect can be appreciable if two of more elements of widely different atomic number are present in high concentration in the specimen, particularly if the lighter element predominates. The concentration of the lighter element is enhanced and that of the heavier element is depressed (Ref. 12).

E. Experimental Results

The interaction effects just described could make data interpretation a formidable or impossible problem when complex samples are to be analyzed, if they occur on a large scale or in a manner which is difficult to treat systematically. To examine this critical matter, sets of

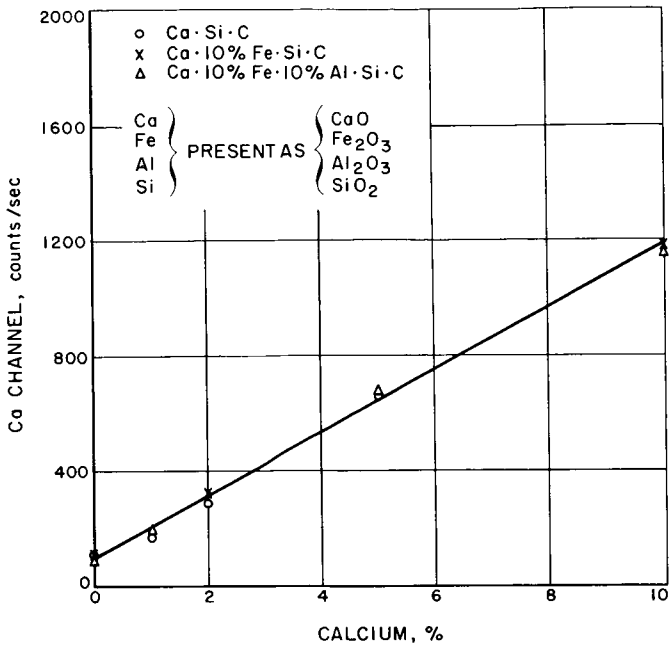

Fig. 11. Dispersive calibration curves of calcium

Figure 10 shows the extent to which a calibration curve of iron in silica is affected by the addition of 10% nickel, calcium, and aluminum. The latter are elements of high, intermediate, and low atomic number respectively, which could be present in appreciable quantity in rock types. All four curves are similar in shape (somewhat concave) and not greatly different in their intensity of response. The calibration curve with added nickel has the lowest intensity, although a comparison of the mass absorption coefficient would have suggested that the Fe-Ca-Si mixture would be the lowest. All points contribute to smoothly varying curves of X-ray emission as a function of changing iron concentration.

Figure 11 shows that the response of calcium is also virtually independent of the presence of elements of greater, lower, and adjacent atomic number. The difference in mass absorption coefficients is more significant for the calcium K-alpha radiation than for the harder iron K-alpha radiation; the similarity of the calcium calibration curves suggests that the effects of absorption will not be excessive. Note that the calcium curves are more linear than those of iron; the intensities for calcium are lower than those of iron, and it is tempting to ascribe the difference in linearity to the radiation detectors. However, the data shown has been corrected for the dead time of the Geiger counters.

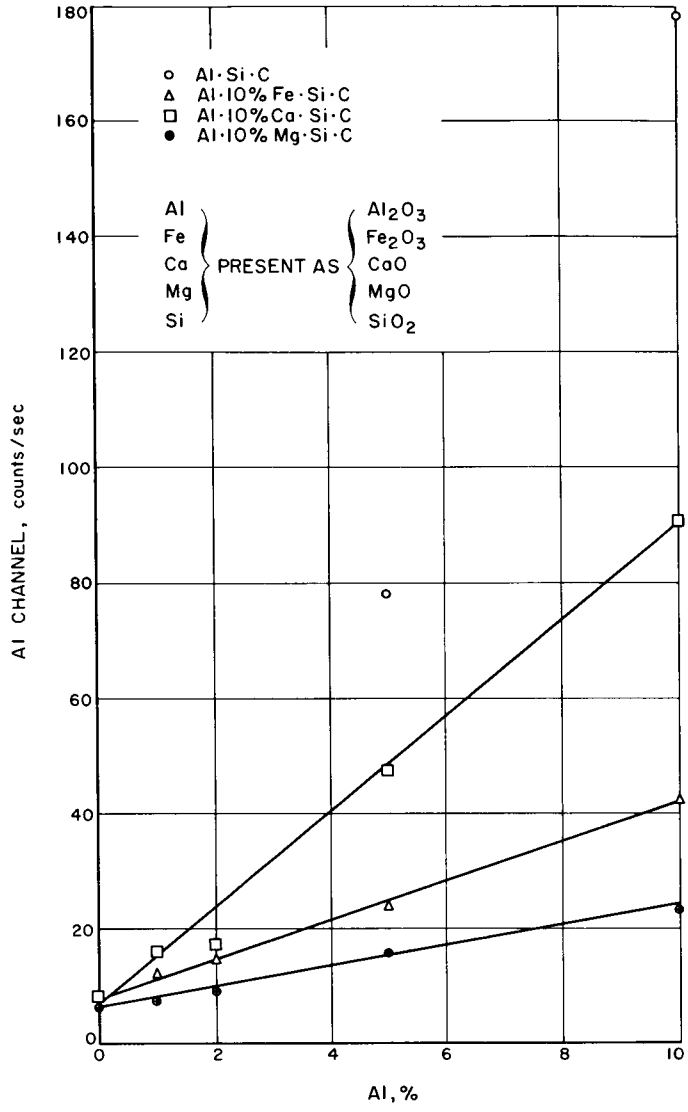

Fig. 12. Dispersive calibration curves of aluminum

Turning to aluminum, striking differences in count rate response make their appearance (Fig. 12). At this wavelength, the absorption coefficients can vary by more than an order of magnitude depending on the atomic number of the absorber. The relative intensities of the curves correspond in each case to the magnitude of the absorption coefficient in the manner expected. At long wavelengths corresponding to the lightest elements that the instrument has been designed to detect (8–12A), the general composition of the rock can be expected to contribute absorption effects requiring correction. In the extreme case shown here, 10% magnesium has the effect of reducing the response from 10% of aluminum by a factor of nine below what it is with magnesium absent.

mixtures containing two, three, and four elements have been prepared and measured on the X-ray Spectrograph. The atomic number range of interest (sodium to nickel) has been divided into three regions: low, intermediate, and high. Tertiary mixtures have been used for the majority of these tests. With silica making up the balance of the sample, the other two elements have been systematically varied in composition from 1–20%. This procedure has been followed for successive pairs of low-low, low-intermediate, low-high, etc., elements. In addition, a few quaternary combinations have been examined to justify the assumption that the conclusions drawn from the behavior of tertiary systems could be extrapolated to multicomponent rock samples. In this manner these tests have involved more than half of the elements provided with dispersive channels in the instrument.

Figures 10–12 show calibration curves obtained from the response of iron, calcium, and aluminum. These elements were chosen to be representative of high, intermediate, and low atomic numbers respectively. Several sets of data are plotted for each element. Each set represents the response of the representative element as a function of its concentration in the mixture. The compositions of each mixture are identified by a symbol and specified according to percentage by weight of the element listed.

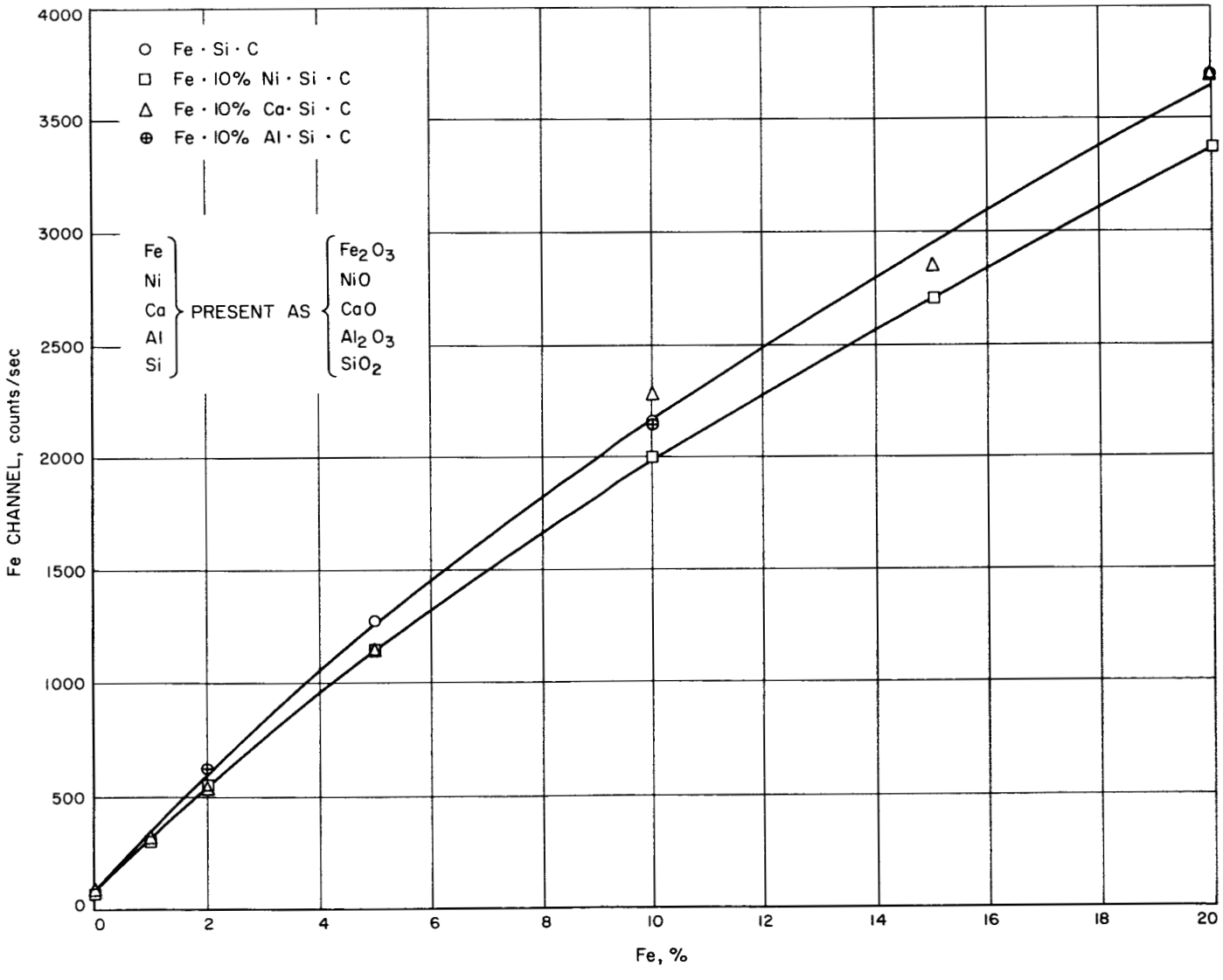

Fig. 10. Dispersive calibration curves of iron

It is significant that in Fig. 10–12, curves of each set show almost identical zero intercepts. This means that although the emitted intensity of an element will be affected by a large change in the overall mass absorption coefficient, the response of the channel in the absence of that element will be essentially invariant; in other words, the *background* count rate will be largely independent of the composition of the sample.

The effect of the matrix has also been examined by keeping the percentage of the element under investigation constant and varying the composition of a second element. Particular attention has been paid in this series of measurements to the critical absorption edge, where a sharp discontinuity exists in the absorption coefficient for a small increase in wavelength. The characteristic X-ray with an energy close to the K absorption edge of an element Z will be far more strongly absorbed by that element than by the element of Z + 1. This strong absorption produced the sharp reduction in response from aluminum in the presence of magnesium seen in Fig. 12.

The critical absorption edge effect is shown in Fig. 13 for the response of a fixed amount of nickel as a function of varying iron concentration, and the response of a fixed amount of aluminum as a function of varying magnesium concentration. In both cases, the absorption wavelength of the element Z is slightly longer than the critical absorption value for the characteristic radiation of Z + 1, so that the fraction of the radiation transmitted through the surface of the sample to the detector decreases with increasing concentration of absorber. The effect is more pronounced for the lower atomic numbers. The existence of this critical absorption edge suggests that for actual rock analysis, magnesium may be a more difficult element to determine than sodium. The higher fluorescent yield and shorter wavelength of the magnesium K_α radiation will be offset by the high value of the mass absorption coefficient of sodium for the magnesium K_α radiation.

In contrast to Fig. 13, Fig. 14 presents the response of iron as a function of the concentration of nickel, and the response of magnesium as a function of the concentration of aluminum. In both of these cases, the adjacent elements have similar mass absorption coefficients for the characteristic X-rays being measured. As a result, absorption effects as a function of changing concentration are comparatively small.

The magnitude of the fluorescence contribution from secondary emission has been sought in the measurements

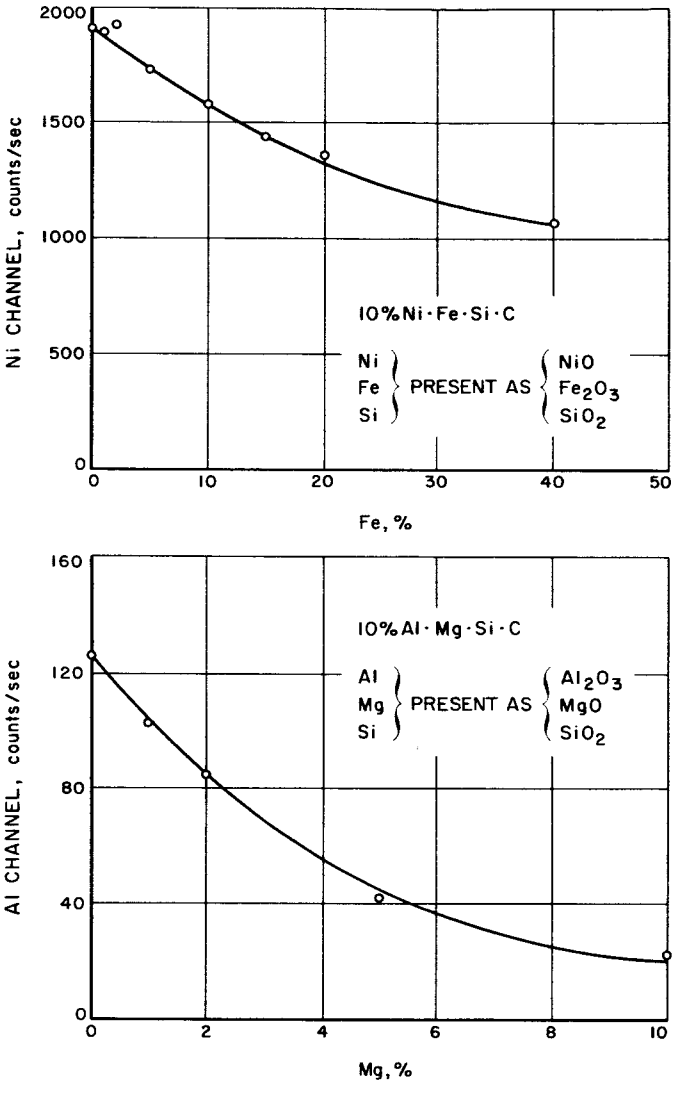

Fig. 13. X-ray absorption in the presence of a critical absorption edge

displayed in Fig. 15. The production of characteristic radiation of shorter wavelength than required for excitation can generate additional radiation through the effect of line or continuum secondary fluorescence, as discussed in Part C of this section. For the case of an excited wavelength close to that being detected (represented by the response of 10% potassium to increasing amounts of calcium), Fig. 15 indicates at best only a slight tendency for enhancement. For the response of 10% calcium to increasing amounts of iron, more favorable for continuum-induced secondary fluorescence, no enhancement is seen. Other curves have also failed to show any evidence of secondary emission. This interelemental effect is therefore negligible for the range of concentrations expected in rock analysis.

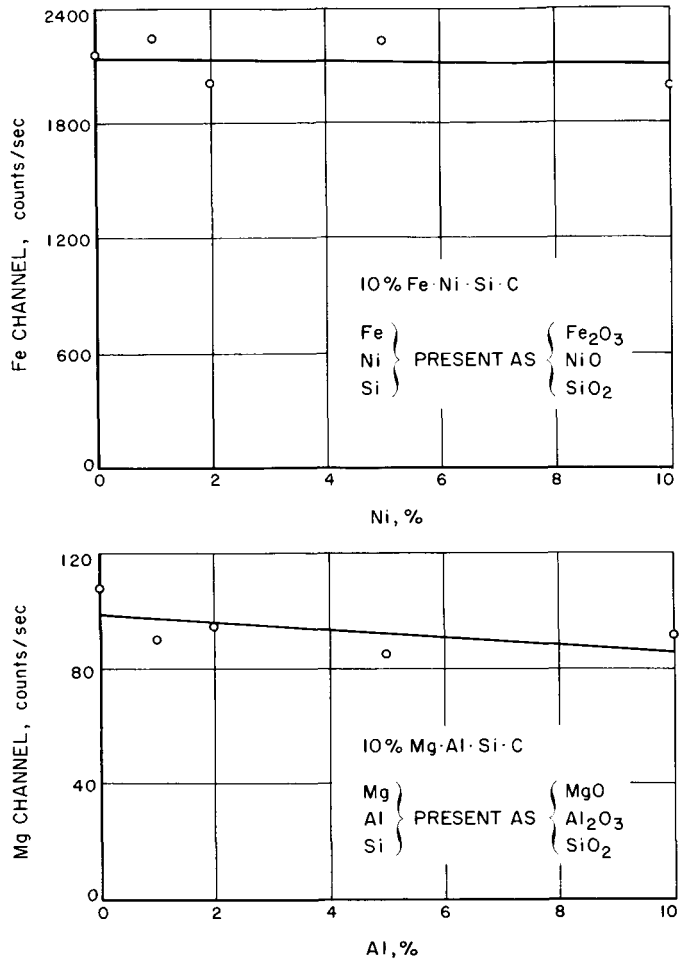

Fig. 14. X-ray absorption in the absence of a critical absorption edge

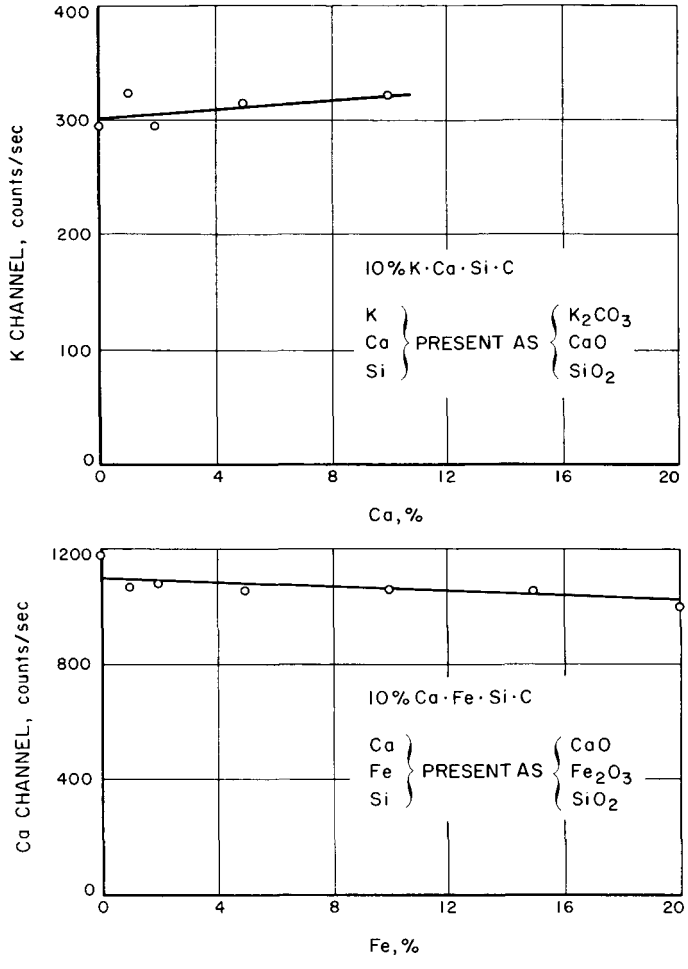

Fig. 15. Interaction measurements for the detection of secondary emission

The atomic number effect described in Part 4 has been evident only in the extreme case of a set of binary carbon-iron samples. The results of this test are shown in Table 7. The measured iron intensity falls below the response expected on the basis of linear proportionality by a factor which increases with the percentage of added carbon. Only if substantial amounts of heavier elements are encountered, e.g., meteoritic iron-nickel, would an atomic number correction be required.

Table 7. Atomic number effect of electron excitation[a]

Added carbon content, %	Measured count rate, c/sec[b]	Expected (linear) count rate, c/sec[b]	Measured/expected
0	3490	3490	—
5	3170	3320	0.96
10	2860	3170	0.90
15	2490	3040	0.82
30	1670	2680	0.62

[a] For Fe Kα radiation in iron–carbon mixtures
[b] Corrected for Geiger counter deadtime

Several of these interaction series have been used as calibration curves in the analysis of unknown mixtures containing the same components. The composition of these unknowns was withheld from those performing the experiment until estimates had been made from the data. Results for two quaternary unknowns are given in Table 8. They show that the Spectrograph is capable of performing quantitative measurements on multicomponent samples.

To summarize, of the four types of interelemental effects discussed, background continuum, absorption, secondary enhancement, and atomic number, only absorption appears to produce significant effects for the

Table 8. Dispersive analysis of quaternary unknowns

Element	Sample I, %			Sample II, %		
	Measured	Prepared	Deviation	Measured	Prepared	Deviation
Fe	7.5	7.9	−5	3.4	3.6	−5
Ca	3.5	3.6	−3	7.9	8.1	−2
Si	40.0	37.4	+7	35.8	36.4	−2
Al	1.7	1.9	−10	3.9	3.0	+30

Note: The Ca results were revised after reassessing the calibration curves; the Si results were obtained by difference.

range of elements and concentrations which apply to rock analysis. The calibration curves have been found to be invariably self-consistent as a function of the element being varied, nearly always consistent with regard to each other, and fully reproducible when sample preparation or instrumental variations were not at fault.

XII. ROCK ANALYSIS

Sections IX and XI have considered the nature and extent of particle and interelemental effects. These studies were made on comparatively simple systems as a necessary preparation for more complex situations. This section will deal with the analysis of actual rock material.

Preliminary tests of the quantitative capability of the X-ray Spectrograph have been made with four rock specimens, a sulfide, a syenite, a gabbro, and a granite. The sulfide ore and syenite rock were supplied by the Nonmetallic Standards Committee of the Canadian Association for Applied Spectroscopy in the form of powdered samples, from a large quantity of material which has been carefully tested for homogeneity. The analysis accompanying the powders also included the number of separate analyses performed. These varied between 3 and 11 for the elements of interest. The composition of these two materials can therefore be considered highly reliable.

The granite and gabbro were ground at JPL from pieces of rock supplied by Dr. R. Speed. No matter how accurate the analysis which accompanied them, the degree to which that analysis is representative of the samples actually tested is less certain than for the sulfide and syenite. The composition of the rocks and the ore is given in Table 9.

The results of measurements in eight dispersive channels of the breadboard are plotted as a function of composition in Fig. 16. Both the original and corrected count rates are shown. The latter values were obtained by simply subtracting, as the background continuum, the response produced in the respective channels by a silica sample, followed by a correction for absorption. The two exceptions to this procedure were silicon and manganese. No continuum correction was applied to the relatively abundant silicon. For manganese, which is adjacent to iron in the periodic table, a weighted continuum of silicon and iron based on their relative percentages in the rock was found to give a more satisfactory background correction than silicon only. The fact that the zero intercept misses the origin for most of the channels indicates that the continuum correction is only an approximation. This is not a problem as long as the relative intensity in each channel is representative of the concentration of the elements which gives rise to it.

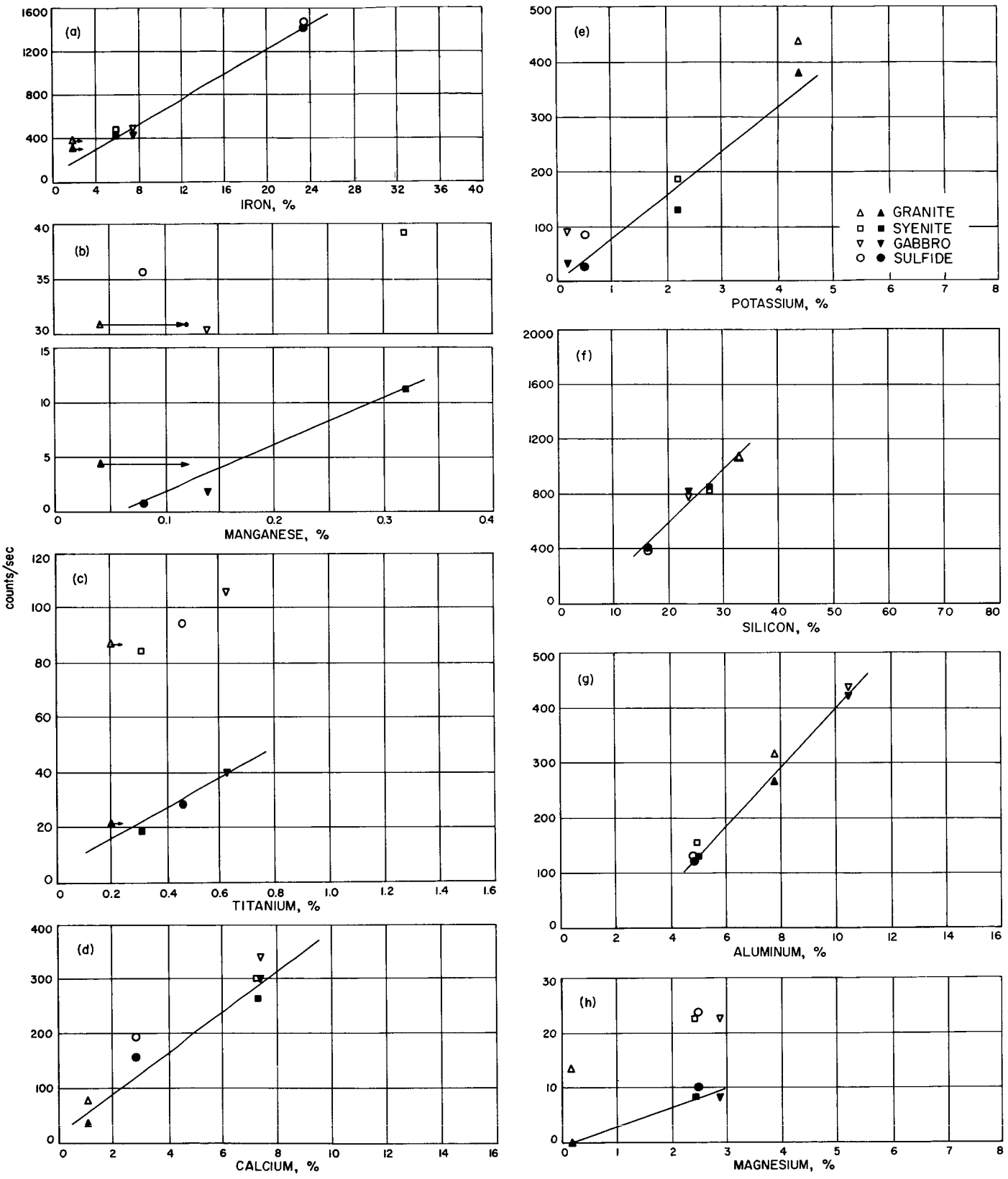

Fig. 16. Rock composition vs. intensity measured on the Lunar Breadboard X-ray Spectrograph. Unshaded symbols represent observed counting rates (adjusted for counter dead time and added carbon); shaded symbols represent observed (adjusted) counting rates corrected for background and enhancement, as required

Table 9. Composition of rocks analyzed on the X-ray Spectrograph

Z	Wt., %			
	Granite	Gabbro	Sulfide	Syenite
O	47.9	46.5	35.6	45.9
Na	3.08	2.22	0.68	2.22
Mg	0.17	2.88	2.46	2.42
Al	7.68	10.4	4.76	4.93
Si	33.0	23.8	16.2	27.7
P	—	—	0.03	0.08
S	—	—	12.1	0.07
K	4.45	0.23	0.51	2.25
Ca	1.00	7.39	2.77	7.31
Ti	0.25	0.63	0.46	0.31
Mn	0.12	—	0.08	0.32
Fe	2.36	7.50	24.0	5.93
U	—	—	—	0.24

That a proportionality between X-ray intensity and concentration does exist can be seen from the corrected count rates of Fig. 16. The linearity of response is in agreement with the observations made on synthesized samples. The absorption correction is small (it averaged 2%, and in only two cases out of about fifty was it more than 10%) but where perceptible, as in the case of aluminum, it has improved the linearity of response. No significant enhancement effects were found.

The point for granite plotted for the composition listed in Table 9 is in poor agreement with a linear response for several of the elements, notably iron, manganese, and titanium. Some of the granite and gabbro powder used in these tests has been subjected to an independent spectroscopic analysis. The results in all three cases, shown by the points of the arrows in Fig. 16a–16c, have brought the value for granite into closer agreement with other points. This indicates that the sample was not representative of the original analysis, rather than the existence of a characteristic particle effect.[b]

To check the performance of the breadboard, the same rock samples were also examined on a commercial laboratory X-ray spectrometer. The results are given in Fig. 17. They are in generally close agreement with those from the X-ray Spectrograph. The response characteristics of the laboratory X-ray spectrometer clearly are shared by the lunar instrument.

In addition to the proportionality between intensity and concentration, and the agreement between the lunar and laboratory instruments, Fig. 16b and 16c demonstrate that the sensitivity of the X-ray Spectrograph for rock analysis extends at least to 0.1 percent. Future improvement in the quality of the results can be expected from longer count periods than were used in these tests, higher beam intensities, crystal and counter design improvements, and the supplemental data available from the nondispersive mode.

A comparison of Fig. 16d and 17d for calcium and Fig. 16h and 17f for magnesium shows that the results from the lunar instrument are more consistent than those from the commercial model! The great efficiency of electron excitation compared to fluorescent excitation more than compensates for the much greater power supplied to the X-ray tube of the laboratory spectrometer. Magnesium and aluminum have low fluorescent efficiencies and their characteristic X-rays are easily absorbed; the excellent results for the two elements are therefore among the most gratifying of these rock tests.

[b] A spectrographic analysis of the gabbro has not improved the linearity of the points for two of the three elements checked. A more comprehensive spectroscopic check of these rocks is pending.

XIII. SUMMARY

The goal of this program has been to establish the functional capability of X-ray spectroscopy as a technique for the compositional analysis of the lunar surface. In that portion of the work reported here, the following results are significant:

1. Stable conditions of sample excitation and X-ray emission can be attained with intense electron beam bombardment.
2. Reproducible and internally selfconsistent results have been obtained in systematic measurements with three and four component specimens.
3. No need has been found for resorting to expedients, such as extreme compaction pressures or sample fusion, which would impose unreasonable requirements on spacecraft support systems.
4. Heterogeneity effects can be significant and are closely related to methods of sample preparation.
5. The nondispersive system provides a useful complement to the dispersive part of the instrument.
6. Data reduction for the dispersive channels is straightforward. Interelemental and continuum effects do not dominate. When they are not insignificant, corrections can be applied successfully.
7. Experiments with rock specimens show that the instrument is capable of quantitative analysis for elements present in major and minor abundance. The same experiments have also demonstrated that the sensitivity of the X-ray Spectrograph will be 0.1% or better for all but the lightest elements of geochemical interest.

APPENDIX

Derivation of Formula for Peak to Background Ratio (Ref. 13, 14)

N = number of counts accumulated

R = detector counting rate

C = concentration of element Z

t = measurement time

R_t = total (signal + background) counting rate

R_s^c = signal counting rate at concentration C (%)

R_b = background counting rate

t_s = sample measurement time

t_b = background measurement time

g_{R_s} = fractional standard deviation of the sample counting rate

n = level of statistical confidence

K = matrix correction factor (for nonlinearity of R_s^c vs. C)

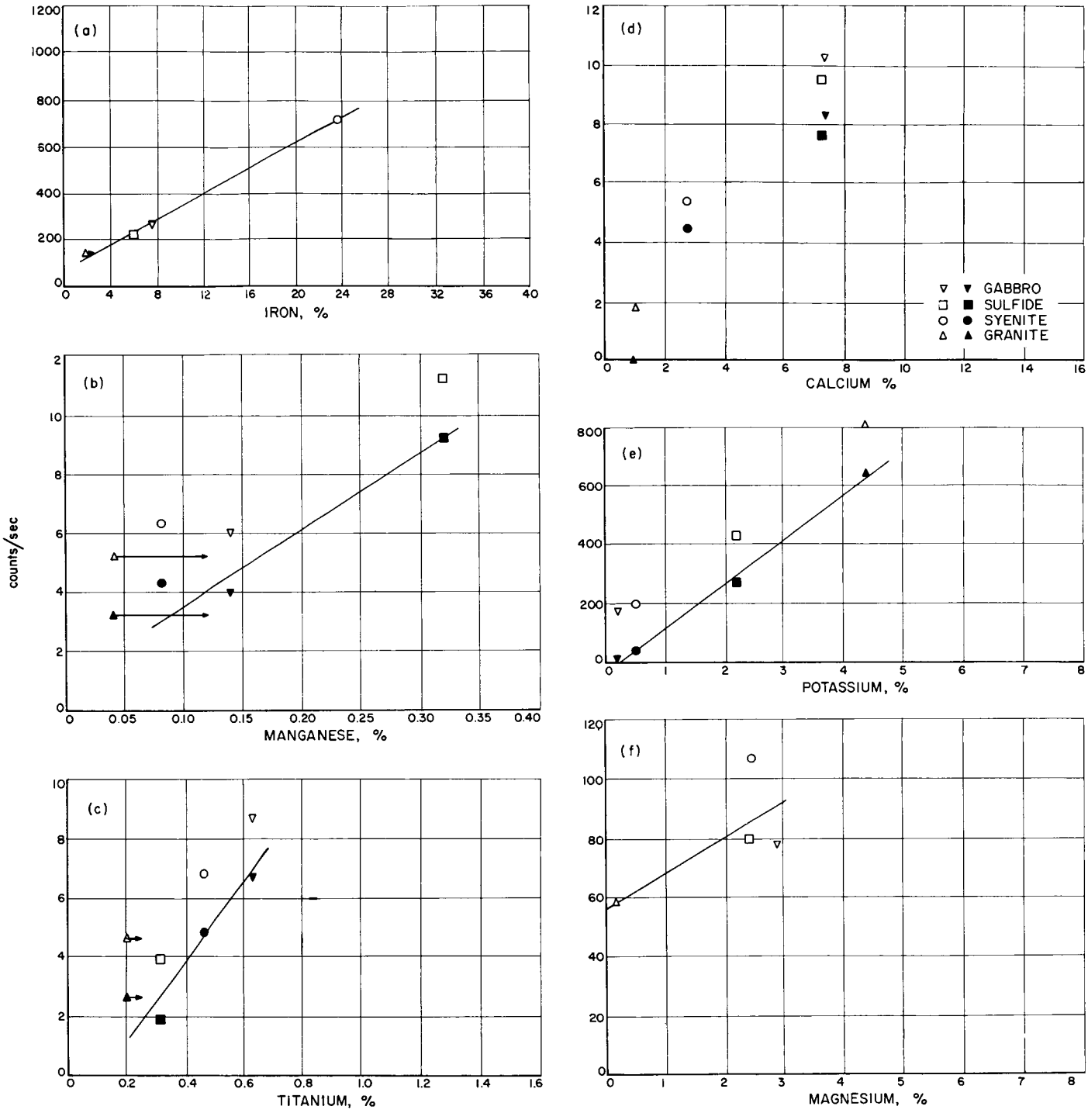

Fig. 17. Rock composition vs. intensity measured on a laboratory X-ray spectrometer. Unshaded symbols represent observed counting rates (adjusted for counter dead time and added carbon); shaded symbols represent observed (adjusted) counting rates corrected for background and enhancement

$$\sigma_N = (N)^{1/2} \tag{1}$$

$$\sigma_R = \sigma_{N/t} = (R/t)^{1/2} \tag{2}$$

$$\sigma_{R_s} = \left(\sigma_{R_t}^2 + \sigma_{R_b}^2\right)^{1/2} = \left(\frac{R_t}{t_s} + \frac{R_b}{t_b}\right)^{1/2} \tag{3}$$

$$g_{R_s} = \frac{\sigma_{R_s}}{R_s} = \frac{(R_t/t_s + R_b/t_b)^{1/2}}{R_s} \tag{4}$$

$$t_b = t_s \left(\frac{R_b}{R_t}\right)^{1/2} \tag{5}$$

and substituting (5) into (4),

$$g_{R_s} = \frac{[R_t + (R_t R_b)^{1/2}]^{1/2}}{(t_s)^{1/2} R_s} \tag{6a}$$

For a certain confidence level, n_σ, and given concentration C,

$$R_s^c = n_\sigma \frac{[R_t + (R_t R_b)^{1/2}]^{1/2}}{g_{R_s} (t_s)^{1/2}} \tag{6b}$$

To reference R_s^c to the case of a pure element, R_s^{100}, use

$$R_s^{100} = \frac{C^{100}}{KC} R_s^c \tag{7}$$

where K corrects for any nonlinearity in the comparative response of the two concentrations.

Equation (6b) can be substituted in (7) to obtain

$$R_s^{100} = \frac{C^{100}}{KC} \frac{n_\sigma}{g_{R_s} (t_s)^{1/2}} [R_t + (R_t R_b)^{1/2}]^{1/2} \tag{8}$$

If R_s^c is not sufficiently low so that $R_t \simeq R_b$, an iterative solution is necessary.

REFERENCES

1. Miller, D. C., and C. F. Hendee, "X-Ray Analysis of the Lunar Surface," paper presented at the National IAS-ARS Joint Meeting, Los Angeles, California, June 13–16, (1961).
2. Adler, I., USGS, private communication, (1962).
3. Philips Space Development; *Progress Report—Spectrometer*, PSD-13-S63-0115, Mount Vernon, New York, January 15, (1963), p. 6.
4. Claisse, F., and C. Samson, "Heterogeneity Effects in X-ray Analysis," *Advances in X-ray Analysis*, Vol. 5, Plenum Press, New York, (1962), p. 335–354.
5. Trombka, J. I., *Least Square Analysis of Gamma-Ray Pulse Height Spectra*, Technical Report No. 32-373, Jet Propulsion Laboratory, Pasadena, (1962).
6. Karttunen, J. O., H. B. Evans, D. J. Henderson, P. J. Markovich, and R. L. Niemann, "A Portable Fluorescent X-Ray Instrument Utilizing Radioisotope Sources," *Journal of Analytical Chemistry*, 36, (1964), p. 1277.
7. Philibert, J., "A Method for Calculating the Absorption Correction in Electron Probe Microanalysis", *X-ray Optics and X-ray Microanalysis*, ed. by Pattee, Cosslett, and Engstrom, Academic Press, New York, (1962), p. 392.
8. Birks, L. S., *Electron Probe Microanalysis*, Interscience Publishers, Inc., John Wiley and Sons, New York, (1963), p. 186.
9. Green, M., "The Target Absorption Correction in X-ray Microanalysis", *X-ray Optics and X-ray Microanalysis*, ed. by Pattee, Cosslett, and Engstrom, Academic Press, New York, (1962), p. 361.
10. Castaing, R., "Electron Probe Microanalysis", *Advances in Electronics and Electron Physics*, 13, (1960), p. 372.
11. Duncumb, P., and P. K. Shields, "Calculation of Fluorescence Excited by Characteristic Radiation in the X-ray Microanalyzer", *X-ray Optics and X-ray Microanalysis*, ed. by Pattee, Cosslett, and Engstrom, Academic Press, New York, (1962), p. 329.
12. Archard, G. D., and T. Mulvey, "The Effect of Atomic Number in X-ray Microanalysis", *X-ray Optics and X-ray Microanalysis*, ed. by Pattee, Cosslett, and Engstrom, Academic Press, New York, (1962), p. 393.
13. Birks, L. S., *X-Ray Spectrochemical Analysis*, Interscience Publishers, Inc., John Wiley and Sons, New York, (1959), p. 53.
14. Overman, Ralph T., and H. M. Clark, *Radioisotope Techniques*, McGraw-Hill Book Co., New York, (1960), p. 117.

ACKNOWLEDGMENT

R. A. Shields performed the bulk of the tests described in this Report. He is also to be credited with mechanical modifications to the breadboard and for the design of special test fixtures required during the program. G. R. Wright made extensive contributions to the proper operation of both the breadboard and laboratory support electronics. R. E. Parker was responsible for the computer analyses and assisted in the reduction of much of the data.

It is a pleasure to acknowledge valuable conversations with Dr. Herbert Schnopper.

Professor Harrison Brown has been designated as Experimenter for this program, which NASA has supported as part of the *Surveyor* project.